JGR Atmospheres

RESEARCH ARTICLE
10.1029/2018JD029457

Special Section:
Bridging Weather and Climate: Subseasonal-to-Seasonal (S2S) Prediction

Quantifying Regional Sensitivities to Periodic Events: Application to the MJO

A. M. Jenney[1], D. A. Randall[1], and E. A. Barnes[1]

[1]Department of Atmospheric Science, Colorado State University, Fort Collins, CO, USA

Abstract As the forecasting community works toward skillfully applying the predictive power of periodic events, it is increasingly useful to quantify regional sensitivities to their influence. We have developed an index to quantify these regional Sensitivities To the Remote Influence of Periodic EventS (STRIPES). Here, periodic events are climate phenomena that smoothly evolve through their life cycles, such as the Madden-Julian Oscillation (MJO). The STRIPES index compiles the information obtained through composite analysis of variables after a periodic event into a single number, which includes information about the life cycle of the event, and for a range of lags with respect to each stage of the event. The STRIPES index quantifies the strength and consistency of a region's response to the remote event. Because the index can be computed for a single point, it can be plotted on a map to show regional variations. We demonstrate the utility of the STRIPES index by applying it to observations of daily geopotential height, maximum temperature, minimum temperature, and precipitation totals for winters between 1974 and 2017. Results for geopotential height show strong sensitivities in the extratropics, indicative of the MJO's remote teleconnections. Results for surface stations over eastern North America highlight regions of enhanced sensitivity that agree well with previous studies. This sensitivity is robust in the sense that it is detectable and significant at the level of individual weather stations. The STRIPES index values for the MJO over North America are generally larger for daily maximum than for daily minimum temperature.

Key Points:
- A new method is developed to quantify regional sensitivity to periodic weather events
- The method is applied to global geopotential heights and North American weather stations
- Temperatures at individual North American stations are significantly sensitive to the MJO

Supporting Information:
- Supporting Information S1

Correspondence to:
A. M. Jenney,
andrea@atmos.colostate.edu

Citation:
Jenney, A. M., Randall, D. A., & Barnes, E. A. (2019). Quantifying regional sensitivities to periodic events: Application to the MJO. *Journal of Geophysical Research: Atmospheres*, *124*, 3671–3683. https://doi.org/10.1029/2018JD029457

Received 8 AUG 2018
Accepted 8 MAR 2019
Accepted article online 18 MAR 2019
Published online 1 APR 2019

1. Introduction

Decision-makers who use weather and climate information can benefit tremendously from skillful forecasts in the 10- to 30-day range (White et al., 2017). For example, the serious human impacts of extreme weather events, such as heat waves, have prompted the agricultural, public health, and energy sectors to request and take advantage of extended-range forecasts of these events in order to save lives and money (Hudson et al., 2015). Ongoing efforts to improve weather forecasts at this time scale are motivated by growing evidence that improvements are indeed possible (Mariotti et al., 2018; Vitart et al., 2017)

Much of the potential for extended-range midlatitude weather prediction is linked to tropical deep convection (Hoskins, 2013; Zhang, 2013). The Madden-Julian oscillation (MJO; Madden & Julian, 1971, 1972) and other periodic weather events (PWEs) have repeatedly been shown to enable subseasonal-to-seasonal (S2S) prediction skill in midlatitudes (e.g., Black et al., 2017; DelSole et al., 2017; Johnson et al., 2014; Jones et al., 2011; Matsueda & Takaya, 2015; Mundhenk et al., 2018; Lin et al., 2010a; Slade & Maloney, 2013). Deep convection associated with the MJO excites Rossby waves that can travel poleward to both influence the immediate circulation (Hoskins & Karoly, 1981) and help maintain longer-lived climate modes such as the Pacific-North America or North Atlantic Oscillation patterns (Cassou, 2008; Higgins & Mo, 1997; Johnson & Feldstein, 2010; Lin et al., 2009; Mori & Watanabe, 2008; Moore et al., 2010), which themselves are important for extended-range weather prediction (Ferranti et al., 1990; Johansson, 2007).

As the forecasting community works toward skillfully applying the predictive power of PWEs (Hoskins, 2013), it will be important to quantify regional sensitivities to these events. Indeed, the results of various methods have already demonstrated regional variations in midlatitude sensitivity to tropical forcing. The strength and location of observed extreme temperature events and the skill of their prediction appear to vary with MJO phase (Diao et al., 2018; Matsueda & Takaya, 2015). The frequency and intensity of precipitation over parts of North America are demonstrably sensitive to the intensity and location of tropical intraseasonal convection (Jones & Carvalho, 2014; Moon et al., 2013; Zhou et al., 2012). Furthermore, verifications of both

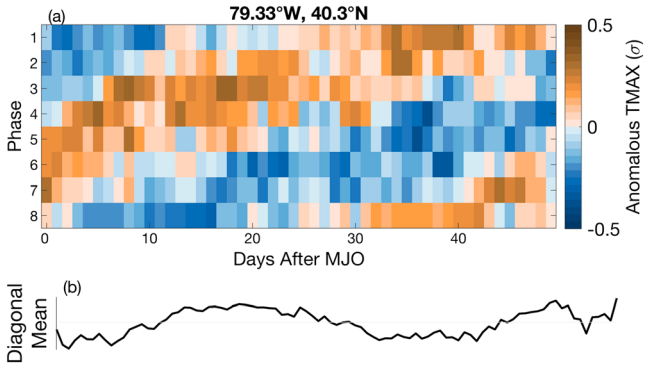

Figure 1. (a) Composited daily maximum temperature anomalies at a weather station indicated by the coordinates (in southwest Pennsylvania) after independent MJO days. The data have been standardized so that anomalies are in units of standard deviations. (b) Resultant vector when diagonal averages are taken of (a) along lines with a slope of 6 days per phase. TMAX = maximum temperature; MJO = Madden-Julian oscillation.

statistical (Cassou, 2008; Johnson et al., 2014; Mundhenk et al., 2018; Slade & Maloney, 2013; Zhu & Li, 2017) and dynamical (Jones et al., 2011; Lin et al., 2010b; Matsueda & Takaya, 2015; Vitart & Molteni, 2010) forecast models trained or conditioned on the MJO reveal regional variations in model skill and thus hint at regional variations in teleconnection strength.

The MJO does not impact all middle- and high-latitude regions equally. The same is likely true for other PWEs with remote teleconnections. Identifying regional variations in climatological teleconnection signal strength is useful for application to S2S predictability endeavors and for climate model evaluation. However, the results of methods heretofore used to identify these regions are difficult to present concisely. One commonly employed technique involves first subdividing a PWE into phases and then compositing a variable of interest after each phase. This method has been used extensively to evaluate the average state of the atmosphere following an MJO event (e.g., Bond & Vecchi, 2003; Becker et al., 2011; Cassou, 2008; Curtis & Gamble, 2016; Donald et al., 2006; Garfinkel et al., 2012; He et al., 2011; Henderson et al., 2016; Jones et al., 2004; Lin et al., 2010a; Moon et al., 2011; Matsueda & Takaya, 2015; Roundy et al., 2010; Riddle et al., 2013; Zhou et al., 2012). The results of such analyses are typically displayed using maps, each showing the composited variable at some lag after some specific time in the PWE's life cycle. Many maps are needed to show the composite response over the life cycle of the PWE, and even more are required to investigate how the response varies with lag. While overwhelmingly informative, this type of data presentation can be difficult to interpret, especially without a very specific question in mind.

Compositing methods can be presented much more succinctly if one dimension, such as space, is removed, as in Figure 1a. Here, the composited daily maximum temperature (TMAX) at a weather station in southwest Pennsylvania is presented for all phases of the MJO for lags ranging from 0 to 50 days after the occurrence of MJO events. This approach presents the composited behavior of a variable at a specific location, for a large number of lags, and over the entire life cycle of the PWE. Drawbacks of composites like Figure 1a include the need to specify a location before construction. Thus, in order to identify the large-scale mechanisms responsible for any apparent teleconnections, composites such as that shown in Figure 1a are insufficient, and maps are again required.

Here, we present the "Sensitivity to the Remote Influence of Periodic EventS (STRIPES)" index, which concisely quantifies the magnitude and consistency of a region's response to the remote influence of PWEs. The STRIPES index offers an advantage over other types of compositing methods, because it compiles the two dimensions of temporal information (PWE phase and lag after the PWE) into a single numerical value–something not possible with composite maps. As a demonstration and proof of concept, we apply the STRIPES index to surface weather observations in North America and global geopotential heights after the MJO.

2. Data and Methods

2.1. Data

For our demonstation of the STRIPES method, we use daily surface observations of TMAX, minimum temperature (TMIN), and precipitation totals (PRCP) from the Global Historical Climatological Database-Daily (Menne et al., 2012). We consider only weather stations in North America that have at least 50% of data for at least 50% of winters (the entire months of December, January, and February). This leaves 6,580, 6,589, and 8,552 available stations for TMAX, TMIN, and PRCP, respectively. Most station data are in fact much more complete; for each variable at least 72% of stations are at least 70% complete for at least 70% of winters. Geopotential height and precipitable water data are from the National Centers for Environmental Prediction/National Center for Atmospheric Research Reanalysis 1 (Kalnay et al., 1996). We use data from the years 1974 to 2017. The data are converted to anomalies by removing the long-term mean, the first three annual harmonics, and any linear trend.

2.2. MJO

We characterize the MJO using the Real-time Multivariate MJO index (RMM, defined by Wheeler & Hendon, 2004). MJO phases are defined by the angle between the first two principal components of the RMM index (RMM1, RMM2), which determines where in a two-dimensional phase space that has been divided into eight equal sections a given day falls.

For all composites, we use independent MJO phase days to ensure that composites do not give extra weight to slower-moving MJO events (i.e., MJO events that spend more consecutive days in a given phase). For a given phase, we choose independent days to composite over by first grouping all occurrences of an MJO phase into events. We define an event as any occurrence of consecutive days of an MJO phase. Disregarding all days below an amplitude threshold ($\sqrt{\mathrm{RMM1}^2 + \mathrm{RMM2}^2} < 1$), we then choose the first occurrence of the MJO phase in each event to construct composites. This leaves a mean number of 121 independent days per phase (with a range of 98 to 139) that are used to construct composites. The results are qualitatively similar when all days within an MJO phase, instead of independent days, are used for composites (see supporting information Figures S1–S3).

2.3. Composites

We construct two-dimensional lagged composites (henceforth, "2-D composites") of observations after active MJO days (see Baggett et al., 2017; Johnson et al., 2014; Mundhenk et al., 2018; Zheng et al., 2018). Composites are created for each station (grid point) for surface (reanalysis) data. All station and reanalysis anomalies have first been standardized by subtracting their individual winter means (over all winters) and dividing by their winter standard deviations, so that regions with different climatological variabilities are comparable. Standardization desensitizes the STRIPES index to the climatological variance of the variable at that station or grid point. Figure 1a shows an example 2-D composite for TMAX at a station in southwest Pennsylvania. The figure shows diagonal stripes of the same sign, which are oriented from bottom left to top right and that have a slope of about 6 days per phase. These stripes are consistent with propagation of the MJO (Wheeler & Hendon, 2004). An organized response to the MJO is evident even when the MJO precedes the TMAX anomaly by as much as 50 days. This is quite remarkable: Although the magnitudes of the composites within the stripe are small, sensitivity of TMAX to the MJO is evident even at a single weather station, where no area or temporal smoothing has been applied. Additionally, diagonal stripes indicating sensitivity to the MJO are clearly discernible despite averaging over more than 40 years of MJO events. We choose to omit showing the significance of composites at a given lag and phase because our focus is on the stripe patterns within these composites, not on the value or sign of the composite response to the PWE at a given point.

3. Calculation of the STRIPES Index

Two-dimensional composites, such as those shown in Figures 1a and 2a, present information about the time evolution of the local response to a remote forcing by a PWE. Of note is the appearance of diagonal stripes, oriented from bottom left to top right. When these stripes alternate sign from left to right and have a slope consistent with the periodicity of the PWE, they provide support for a physical link between the PWE and the composited variable. Compositing over many events helps to filter out variability not due to the PWE and isolates consistencies over many events. In these cases, the appearance of diagonal stripes provides even stronger evidence for a systematic, physical link between the PWE and the composited variable.

The calculation of the STRIPES index is based on these 2-D composites, and aims to quantify the amplitude of the stripes. An area that is not sensitive to the PWE will have 2-D composites that appear noisy, have weak overall amplitudes, and contain no systematic stripes. Conversely, areas that respond to the PWE with larger magnitudes and more consistency will have prominent, and sometimes multiple, stripes.

The STRIPES index can be technically understood as the variance of a one-dimensional vector of values obtained as averages taken along the diagonals of the 2-D composites. Figure 2 is a synthetic example intended to aid in the interpretation of this algorithm. Here, a synthetic 2-D composite has been drawn, with amplitudes reaching 0.25 standard deviations, which decrease by 30% at a lag of 50 days. We include this decrease in amplitude with lag to make the synthetic composite more realistic.

Diagonal averages are taken along lines with a slope consistent with the periodicity of the PWE. In the artificial example shown in Figure 2, we choose a slope of 6 days per phase, because the MJO spends about

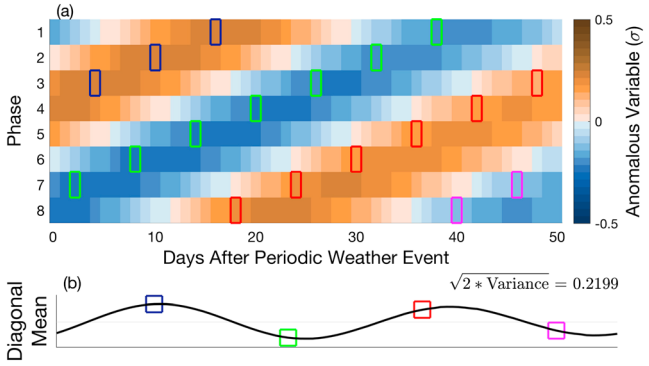

Figure 2. (a) Synthetic composited variable after many ostripeccurrences of an active periodic weather event. Maximum amplitude anomalies are 0.25 standard deviations, and decrease to 70% of that at 50 days. The STRIPES index is constructed by taking averages of composites along the diagonal along which the stripes occur, and using the value of each average to construct a vector. (b) The resultant vector for the synthetic data, with the average stripe amplitude ($\sqrt{2 * \text{variance}}$) shown in the top right. Colored boxes at specific points of the curve demonstrate the value of the average taken along the diagonal indicated by the line of similarly colored boxes in (a). The slope along which the diagonal averages are taken is 6 days per phase. STRIPES = Sensitivities To the Remote Influence of Periodic EventS.

6 days in each RMM phase before transitioning to the next (Wheeler & Hendon, 2004). Four of these diagonal lines and their sums are visualized in Figure 2. Boxes of the same color lie along one of these diagonal lines, and each box indicates the point used in that line's diagonal average. These points are separated in time by 6 days. For each diagonal line, only 1 day per phase is used in averages. Figure 2b shows the one-dimensional vector that results when diagonal averages of Figure 2a are taken. The colored squares on the curve indicate the averages for the diagonal lines indicated by boxes of the same color in Figure 2a. The sinusoidal shape of the one-dimensional vector of diagonal averages is a result of robust stripes of alternating sign in the 2-D composite.

After the diagonal averages are taken, the variance of the resulting one-dimensional vector is calculated. For a perfect sine or cosine function, the variance is one half the square of the amplitude. Thus, we can transform the variance into an amplitude by taking the square root of twice its value. This transformation helps convert the index into a number that coveys the average magnitude of composites along its diagonal stripes. The number that results from this transformation is, in essence, the STRIPES index. For the synthetic composite shown in Figure 2, the amplitude that results is 0.2199. This is roughly the magnitude of the composites within the stripes (0.25), but is smaller because of the specified 30% decrease in amplitude with lag. If maximum amplitudes along stripe axes in Figure 2 were 0.25 everywhere, then the STRIPES index for this composite would also be 0.25. The STRIPES index for Figure 2 would be lower if one or multiple of its diagonal stripes was composed of an equal number of positive and negative points, such that the diagonal average of that line was near zero. The STRIPES index has a single value at each geographical point, meaning it can be plotted on a map to show regional variations in apparent sensitivity to a PWE. This makes it particularly useful.

While the steps described above create the fundamental STRIPES index, we take additional steps to remove minor sensitivities. Nonetheless, the STRIPES index is robust as described, and gives qualitatively similar results to those with the following additional steps (see Figures S4–S6). First, we repeat the calculation of the index *N* times, where *N* is the number of phases used to subdivide the PWE. In each iteration, the PWE's subdividing phases are shifted before computing the variance of diagonal averages. This gives *N* values for the final variance, which are then averaged together to get a single value for the variance. The shifting captures those stripes in the composites that are due to periodic behavior (i.e., returning to the beginning of the event after completing a cycle). For example, in one iteration, instead of the ordinate axis of the composite shown in the top panel of Figure 2 running from phases 1 to 8, it runs from phases 5 to 8, and then 1 to 4. Inspection of Figure 2a shows that stripes appear to extend beyond phase 8 or before phase 1. Each iteration of this calculation contributes a variance value. The STRIPES indices presented in section 4 use the average of the eight variances obtained with this shifting. Second, we average together the four variances obtained using slopes between 4 and 7 days. We do this to account for the variability in MJO periodicity (e.g., Hendon & Salby, 1994). The final result is a single variance, which is then transformed into an amplitude that quantifies the magnitude and consistency of a region's response to the remote influence of PWEs. This number can be interpreted as the average value (in standard deviations) of composites along the stripes in the 2-D composites. We calculate the significance of the STRIPES index at each weather station using a bootstrap method, which is described in the appendix.

The STRIPES index has a lower bound of zero and no upper bound. Diagonal stripes in the 2-D composites that are not consistent with the periodicity of the PWE will not contribute positively to the index. The STRIPES index is insensitive to the location of a stripe in the 2-D composites. For example, a 2-D composite like the one shown in Figure 2a, but with stripes that are in quadrature with those of Figure 2a, will have the same STRIPES index as Figure 2a. The STRIPES index will have a larger magnitude if, for a given PWE, there are multiple stripes (e.g., if a PWE excites an opposite-signed response every half cycle) or if stripes are particularly strong. Although multiple stripes can appear in the 2-D composites for PWEs with a shorter period, the index is not sensitive to the periodicity of the PWE. Using the variance as a measure of stripe magnitude helps to amplify actual stripe signals while suppressing noise.

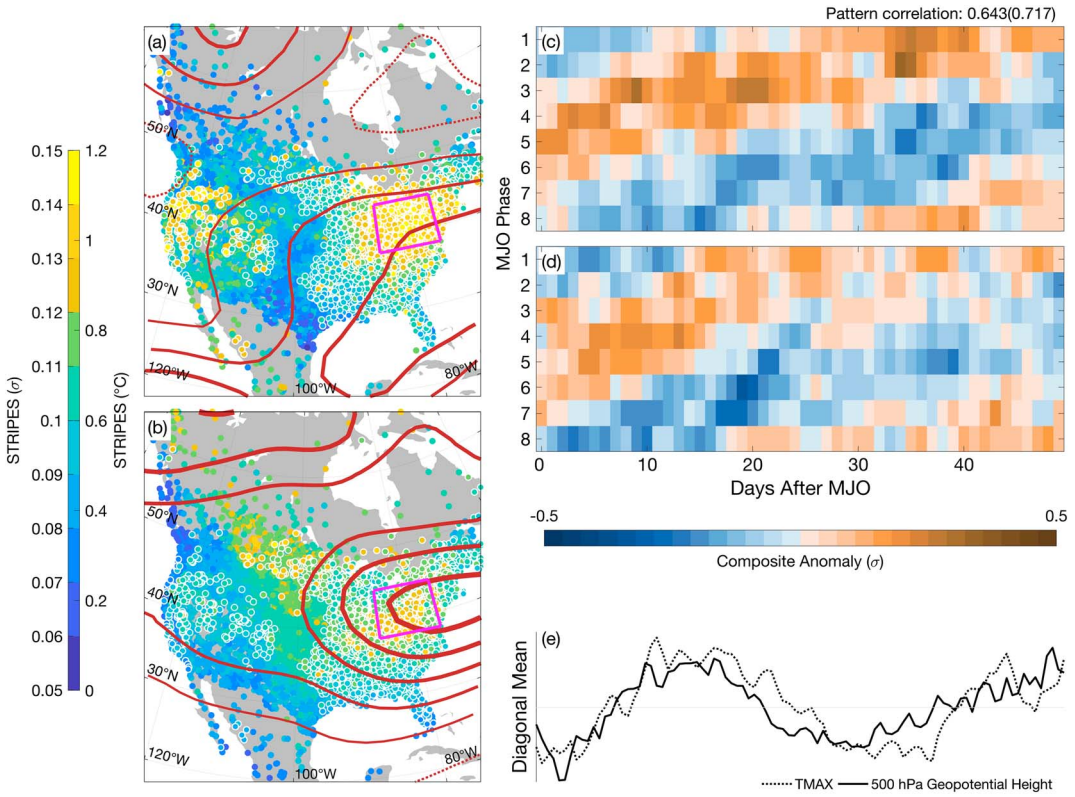

Figure 3. (a) STRIPES index for North American weather stations (each point on the map is a unique weather station) for maximum temperature (TMAX; points) and 500-hPa geopotential height (contours) after the MJO for the years 1974–2017 in (a) standard deviations. Contours start at 0.06 (dotted) and increase in value with thickness by 0.02 (solid). (b) As in (a), but STRIPES is shown in degree Celsius for TMAX and meters for geopotential height. Contours start at 2 m (dotted) and increase in value with thickness by 2 m (solid). (c) A 2-D composite of TMAX for the region enclosed by the magenta box (33–44.5°N, 75.5–86°W). (d) A 2-D composite of 500-hPa geopotential height for the region enclosed by the magenta box. (e) Diagonal means of the composites using a slope of 6 days per phase. STRIPES = Sensitivities To the Remote Influence of Periodic EventS; MJO = Madden-Julian oscillation.

The STRIPES index can be applied to a variety of PWEs. While the specific values given in the methods described here and the application of the index in section 4 are for the MJO, the same approach can be applied to any other PWE whose life cycle is smoothly periodic and can be subdivided into distinct phases, such that 2-D composites like the one shown in Figures 1a and 2a can be constructed. For example, consider a PWE that has a periodicity of 24 days. If eight phases are still being used to subdivide the event, then a slope of about 3 days per phase should be used in diagonal averages rather than 6, as was shown here. Similarly, if a PWE with a period similar to that of the MJO is only being subdivided into four phases rather than eight, then a slope of about 12 days per phase should be used in diagonal averages.

4. Application of the STRIPES Index to the MJO

We apply the STRIPES index to observations at North American weather stations and to global 500 hPa geopotential heights following MJO events to quantify the magnitude and consistency of local responses to the MJO.

4.1. TMAX

Figure 3a shows the winter STRIPES index for daily TMAX. STRIPES for geopotential height at 500 hPa are overlaid as red contours. Units of the STRIPES index are in standard deviations, so that the variability of a region's temperature or geopotential height is not encoded in the magnitude of STRIPES. However, the STRIPES index can also be presented in variable units to get a sense of the magnitude of the variability associated with the MJO in measurable quantities. We show this for TMAX and 500-hPa geopotential height in Figure 3b, where the STRIPES index at each point has been multiplied by the local standard deviation.

A strong hot spot for local modulation of TMAX by the MJO is over eastern North America, as shown by the large magnitudes of the STRIPES index over this region in Figures 3a and 3b. This hot spot also appears in previous studies employing alternate methods. Zheng et al. (2018) also identified strong MJO covariability over eastern North America in winter. Additionally, composites of winter near-surface air temperature and geopotential height anomalies after RMM phases of the MJO have large magnitudes with strong significance over eastern North America relative to other North American regions (Baxter et al., 2014; Matsueda & Takaya, 2015; Schreck et al., 2013; Zhou et al., 2012). Finally, the MJO appears to be linked with the skill of temperature forecasts particularly over eastern North America (Johnson et al., 2014; Matsueda & Takaya, 2015).

Figure 3a indicates that the region of elevated surface TMAX sensitivities is collocated with a tongue of high sensitivities in 500-hPa geopotential height stretching westward from the Atlantic Ocean, suggesting that MJO-induced circulation anomalies over the East Coast play a key role in the MJO-coincident TMAX variations at the surface. This is expected: The remote MJO must communicate its signal to North America through a control on larger-scale circulations in order to influence weather at the surface. Seo et al. (2016) show that low-level horizontal advection is the dominant process through which the MJO influences temperatures over this region. Figure 3c shows the 2-D composite for TMAX area averaged (as in McKinnon et al., 2016) over the region enclosed by the magenta box in Figures 3a and 3b. Warm anomalies over this region occur around 10 days after MJO Phase 3. When this occurs, Seo et al. (2016) show that the circulation pattern characterized by an anomalous low over Alaska and high over the Atlantic encourages warm air advection over eastern North America, which is situated between the two circulation anomalies. Figure 3e, which shows the diagonal means of the 2-D composites for TMAX and 500-hPa geopotential height (Figure 3d) for the boxed eastern North America region, shows this pattern. Anomalous warm temperatures tend to follow maxima in anomalous geopotential height; that is, warm (cold) air advection ramps up when the center of the anomalous high (low) associated with the Rossby waves excited by the MJO propagates just east of the region. Thus, for a given point, there is some time in between maxima (minima) in geopotential height and subsequent near-surface temperature maxima (minima).

Figures 3a and 3b indicate that western North America, especially along coastal California, also displays significant sensitivity to the MJO. Although weaker in amplitude than eastern North America, this is a region that has been previously shown to covary with the MJO (Baxter et al., 2014; Johnson et al., 2014; Schreck et al., 2013; Zhou et al., 2012) and more significantly so when finer resolution temperature data are used (Baxter et al., 2014; Zhou et al., 2012).

4.2. TMIN

The spatial pattern of TMIN sensitivity to the MJO closely resembles that for TMAX (Figures 4a and 4b). The strongest STRIPES indices are also located over eastern North America, but with weaker magnitudes than for TMAX.

Over land, daily minimum temperature is closely linked with atmospheric moisture (e.g., Hartmann, 1994; James, 1953). Boundary layer temperature minima tend to occur at the end of the night after hours of longwave cooling and no solar energy input. Water vapor is the largest contributor to downwelling longwave radiation (Hartmann, 1994). On nights when column moisture is relatively low, there is less downwelling longwave radiation to counteract the efficient surface longwave emission, effectively permitting lower temperature minima. Conversely, on relatively humid nights increased downwelling radiation from water vapor acts to keep the nocturnal temperature from falling as low as it would otherwise. The STRIPES index contours for standardized precipitable water in Figure 4a show that the strongest sensitivities in precipitable water over North America are over and to the southwest of the Great Lakes region (see Figure S7 for a global map of the STRIPES index for precipitable water). Figure 4 shows composited anomalies of both (c) TMIN and (d) precipitable water for the region enclosed by the magenta box in Figures 4a and 4b. Higher (lower) anomalies in precipitable water are coincident with warmer (cooler) daily minimum temperatures. Here, pattern correlations (indicated by the number at the top right in Figures 3c and 4c) between TMIN and precipitable water are much stronger than those between TMAX and 500-hPa geopotential height. This is likely due to the effect of moisture on TMIN: daily minimum temperatures respond to the amount of moisture present in the column, as discussed previously. Figure 4e confirms that stripes of local maxima and minima in TMIN and precipitable water occur at the same time.

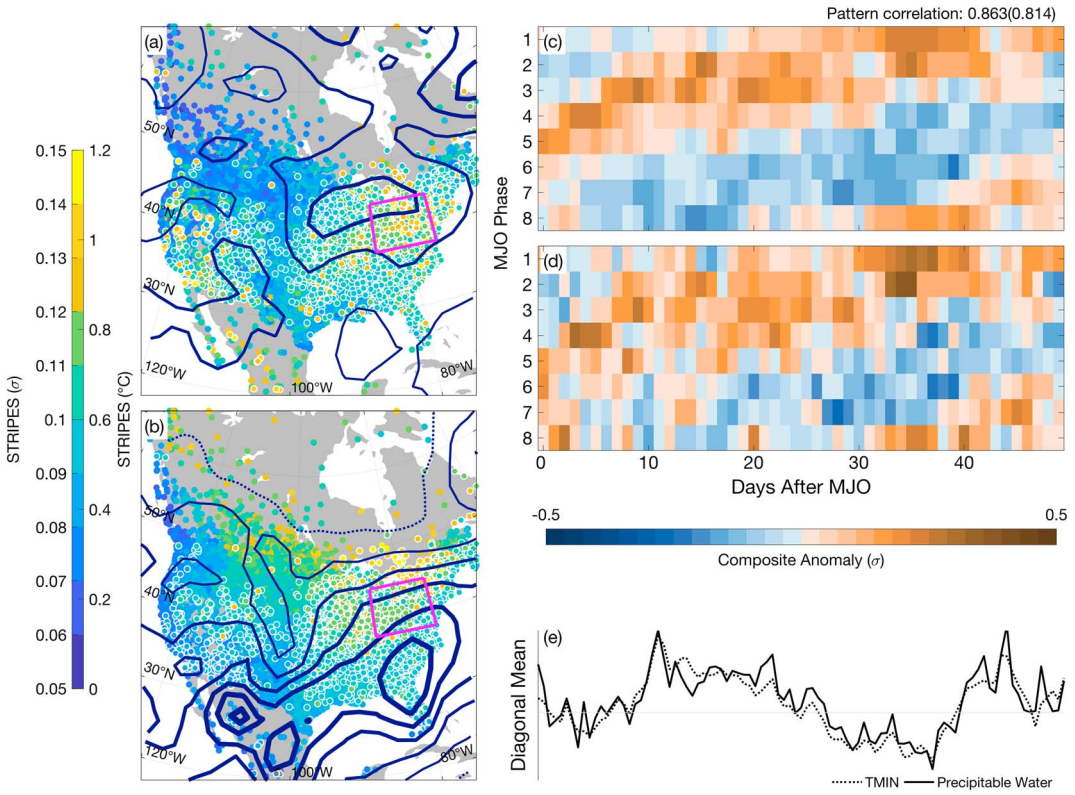

Figure 4. As in Figure 3 but for TMIN and precipitable water instead of TMAX and geopotential height. TMIN = minimum temperature; TMAX = maximum temperature; STRIPES = Sensitivities To the Remote Influence of Periodic EventS; MJO = Madden-Julian oscillation.

Some of the correspondence between TMIN and precipitable water is likely also due to advection. As mentioned previously, the MJO primarily influences the thermodynamics of this region through low-level advection (Seo et al., 2016). Southerly (northerly) advection of mean state temperatures not only brings relatively warmer (cooler) air, but also more (less) humid air. Because of the dynamical link between temperature and moisture, when temperatures are anomalously warm due to warm air advection from the south, absolute humidities are also likely to be elevated for the same reason.

There is an additional hotspot of sensitivity to the MJO for TMIN over the southwest. The significant weather stations are mostly located in the desert southwest, to the north and east of the Gulf of California, whereas for TMAX the significant weather stations in this part of the continent are located further west. This difference is likely due to the presence of the strong hotspot for column moisture near this region (see Figure 4c), to which TMIN is more sensitive. Sensitivity to the MJO over western North America was not detected in the recent analysis of Zheng et al. (2018). In their study, the authors analyzed 2.5° × 2.5° resolution gridded daily means of surface air temperature data. They were likely unable to detect the signal over this region through some combination of the coarseness of the resolution of their data, and their use of daily mean temperature values. Note that only a few western weather stations show significant signals for both TMAX and TMIN.

4.3. Precipitation

Previous work indicates that the MJO strongly modulates winter moisture (Mo & Higgins, 1998), flooding (Bond & Vecchi, 2003), and atmospheric rivers (Mundhenk et al., 2016; Ralph et al., 2010) over the North American Pacific Coastline. Figures 5a and 5b show that weather stations with significant signals in PRCP are clustered in this region, in addition to parts of the southeast. Here, weather stations with standard deviations less than 1 mm/day are plotted as gray points to ignore weather stations with small variability. The recent analysis of Zheng et al. (2018) also indicates strong covariability with the MJO over these two regions, in addition to a peak over the central portion of the continent which was not detected with any significance in our analysis. This may be a consequence of the very noisy nature of precipitation data: Daily station rainfall time series are noisy, have highly asymmetric distributions, and contain a disproportionate number of

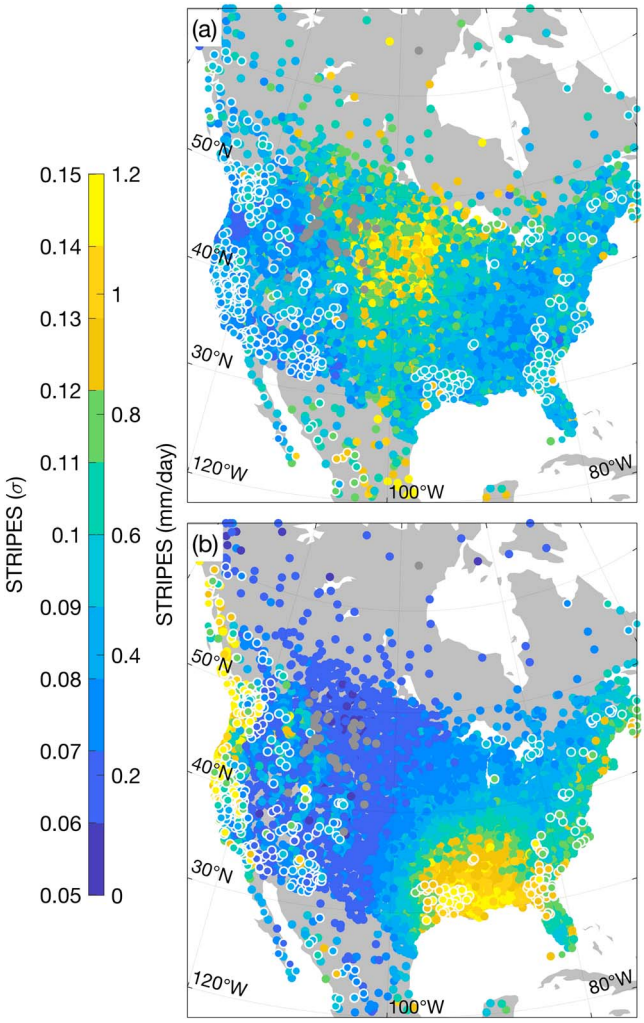

Figure 5. As in Figures 3a and 3b but for PRCP. Stations with standard deviations less than 1 mm/day are plotted as gray circles. PRCP = precipitation totals; STRIPES = Sensitivities To the Remote Influence of Periodic EventS.

zero values. Thus, we expect STRIPES results for this type of data to appear differently than for data like TMAX, for example. Experimentation with a log or hyperbolic sine transformation indeed aided in reducing the skewness of daily rainfall data, but the overwhelming number of zero values is such that the STRIPES index analysis results for PRCP do not change much even with the transformation applied (not shown). Smoothing, for example, by taking 10-day running means or bandpass filtering to retain only the intraseasonally varying component of the signal as in Zheng et al. (2018), or through spatial averaging, may increase the magnitude of the STRIPES index for this type of data.

In standardized values (Figure 5a), the magnitude of the STRIPES index appears to be largest over central North America. However, this central cluster of points is not significant, even when using a relaxed confidence threshold of $\alpha \leq 0.20$ (not shown). Note that when viewed in millimeters per day (Figure 5b), rather than in standard deviations, this region disappears, and the regions shown to be significant now show the largest magnitudes.

4.4. Geopotential Height

We include the STRIPES index for global 500-hPa geopotential heights to give some indication of the global effects of the MJO. As expected, Figure 6a shows that the strongest sensitivities for 500-hPa geopotential height for winter are over the equatorial Indian and Pacific Oceans, where MJO variability is most pronounced. Notable is the pattern of higher STRIPES values in the extratropics. There is strong regionality in the covariability of extratropical geopotential heights with the MJO. For example, the couplet comprised of

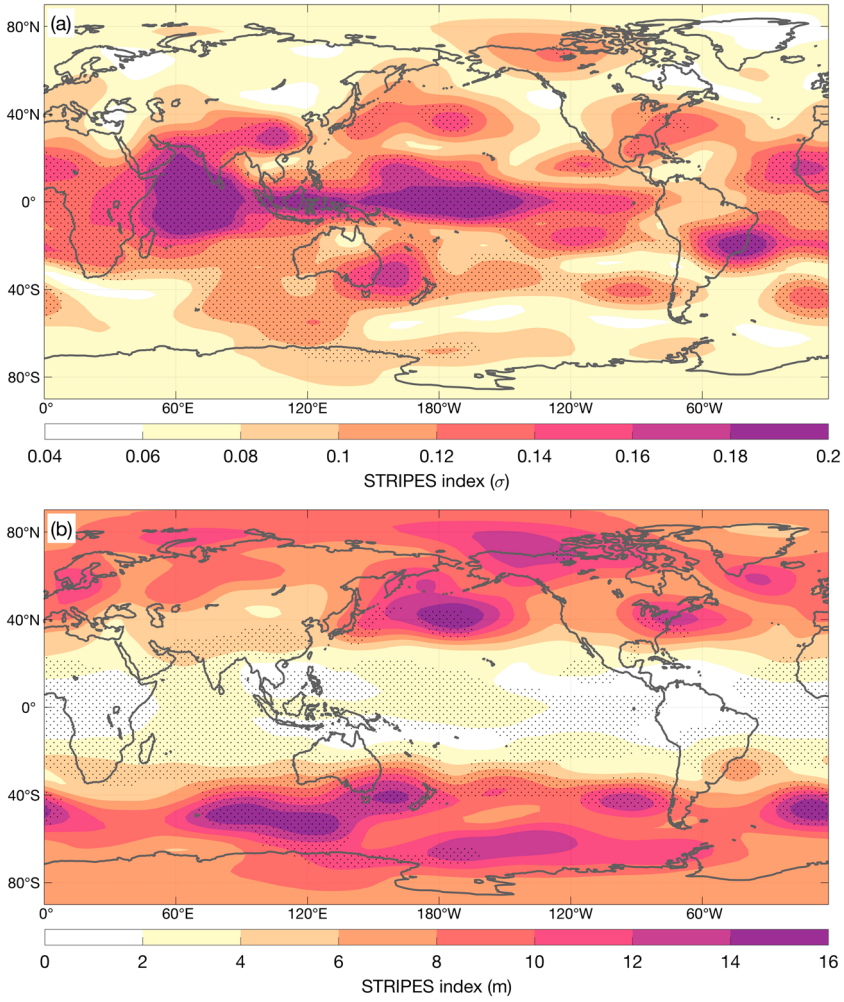

Figure 6. (a) STRIPES index for 500 hPa geopotential height after winter (DJF) MJO events for the years 1974-2017. (b) STRIPES index at each point has been multiplied by its local standard deviation. Stippling denotes significance at $\alpha < 0.05$.

the center just south of the Aleutian Islands and the center over northwest North America is reminiscent of the Pacific-North America pattern, a teleconnection pattern associated with the MJO (Goss & Feldstein, 2015; Mori & Watanabe, 2008; Seo & Lee, 2017). There are many regions whose local circulations show strong covariability with the MJO. While our analysis mainly focused on North America, the circulations of much of Africa, southeast Asia, eastern Australia, and eastern equatorial South America show stronger sensitivities to the MJO than that over North America. In short, the effects of the MJO are widespread.

Figure 6b shows STRIPES indices multiplied by local standard deviations. This translates the STRIPES quantities from units of standard deviation into measurable quantities. Low geopotential height variability in the tropics causes the high sensitivities there to disappear (although they remain significant). Conversely, regions along the Pacific and Atlantic storm tracks are amplified. Maps such as Figure 6 indicate which regions of the globe respond with greater magnitude and consistency to an MJO event.

5. Discussion

We present the STRIPES index as a concise way to quantify the magnitude and consistency of a region's response to the remote influence of PWEs. Its units are in standard deviations and signify the average amplitude of the stripes within a region's 2-D composite. However, the interpretation of the STRIPES index *as an amplitude* relies on the assumption that the one-dimensional vector of diagonal averages assumes a sinusoidal shape. This will only occur when the 2-D composites have stripes of alternating sign, that is, when

the PWE excites opposite-signed responses every half cycle. Thus, some caution is advised in the interpretation of the STRIPES index as an amplitude. For example, the STRIPES index amplitude for 2-D composites characterized by one very strong stripe, but near-zero composites everywhere else will be much lower than the average magnitude of composite quantities within the stripe. Nonetheless, the STRIPES index for such a region will still have a larger value than a similar composite that contains no stripes.

STRIPES indices can be converted back into variable units by multiplying by the standard deviation at each point, as in Figures 3b and 4b. Such a transformation shows how the teleconnection strength over a region translates to measurable quantities. For example, Figure 3b shows that the average magnitude of anomalies in stripes of the 2-D composites of TMAX after the MJO over eastern North America is about 1 °C. Note how the central North American hotspot for PRCP in Figure 5a disappears when this transformation is applied in Figure 5b, while new hot spots over regions with larger climatological variabilities, such as the previously discussed North American Pacific coastline, pop out.

As constructed, the STRIPES index is better suited to data that are symmetrically distributed. Additionally, while there are a number of periodic weather phenomena (e.g., the El Niño–Southern Oscillation, the North Atlantic Oscillation, and the Quasi-Biennial Oscillation) the index requires that the event be somewhat smoothly varying. For example, climate phenomena characterized by irregular or sudden transitions between regime states, such as sudden stratospheric warmings (e.g., Limpasuvan et al., 2004), do not produce diagonal stripes when composites such as the ones shown in Figures 1 and 2 are constructed, and thus, the STRIPES index would not be useful for these phenomena. Instead, the index is designed to work with PWE that somewhat smoothly and consistently evolve through their life cycles. For example, the STRIPES index can be successfully applied to the Quasi-Biennial Oscillation.

Because the STRIPES index allows the concise quantification of the magnitude and consistency of a region's response to a remote PWE, it has strong potential for use in future studies. For example, the STRIPES index could be used in the evaluation of numerical weather or climate models. Comparisons of maps of the STRIPES index constructed using observations to those using global climate models could help in the evaluation of these models. Similarly, comparisons of maps of the STRIPES index to maps of predictability using a forecast model could help identify regions where models are not simulating teleconnections with fidelity. Furthermore, this index could be used to help motivate the development of statistical forecast models for regions where numerical forecast models struggle to simulate observed teleconnections. The STRIPES index may also be applied to quantify seasonal differences in teleconnectivity between PWE and remote regions, or differences due to the influence of other longer-scale PWEs. For example, it has been shown that MJO teleconnections are modulated by El Niño phase (e.g., Henderson & Maloney, 2018; Moon et al., 2011) and the Quasi-Biennial Oscillation (e.g., Mundhenk et al., 2018; Son et al., 2017).

In our application of the STRIPES index to the MJO, we average using diagonal “slopes” of 4 to 7 days per phase. This decision is made to ensure that the diagonal stripes used in the calculation of the index are of MJO periodicity–the MJO is not perfectly periodic, its return time can vary between 20 and 90 days. However, one could conceivably choose a different slope or allow the data to choose the slope that maximizes the variance of the one-dimensional vector of diagonal averages. For PWEs with variable periodicities, this type of analysis could, for example, be used to investigate how PWE propagation speed influences teleconnection signal strength.

The STRIPES index is related to a method devised by Zheng et al. (2018). In that study, the authors create 2-D composites with intraseasonally filtered anomalies and then compute the variance of the result to obtain an index that is qualitatively similar to STRIPES. Their method gives generally similar results to those presented here, although with some differences, particularly for precipitation. The STRIPES index differs from that presented in Zheng et al. (2018) by using unfiltered data, and by targeting propagating anomalies in the 2-D composite (stripes) that are consistent with MJO periodicity through the calculation of diagonal means. The STRIPES index thus selectively amplifies signals in the data that are covariable with the PWE in question, while the method presented in Zheng et al. (2018) attempts to do the same through the use of filtering.

6. Summary and Conclusions

We present the STRIPES index to quantify the observed magnitude and consistency of a region's response to a PWE. The index was designed so that regional variations in teleconnection strength excited by remote PWEs can be quickly and easily quantified.

In the present study, the STRIPES index was applied to investigate the apparent response of 500-hPa global geopotential heights and North American surface weather to MJO forcing. Results for geopotential height show strong sensitivities in the extratropics, indicative of the MJO's remote teleconnections. Results for surface stations indicate an observable link with the MJO over eastern North America, and parts of western North America, that is consistent with previous studies. We additionally show that this link is robust as it both covers a large geographic area and is significant even at the level of individual weather stations (i.e., no temporal or area smoothing is required to detect this link). Furthermore, we show that sensitivities to the MJO not only vary regionally, but also with variable. The magnitude of TMIN sensitivities to the MJO are somewhat weaker than TMAX. The STRIPES index shows promise for use in future studies seeking to apply the predictive power of PWEs. For example, we are using the STRIPES index to investigate the seasonality of MJO teleconnections over the Northern Hemisphere.

Appendix A: Significance Calculation

We calculate the significance of the STRIPES index using a one-tailed bootstrap test with 500 samples at $\alpha < 0.05$. To create our samples, we first separate MJO days into chunks of consecutive days with amplitudes greater than 0.5. We then randomly sample from fall and winter (all of winter plus the 50 days prior to winter) a distribution of days with the same distribution as our chunks. For example, if there are 10 MJO chunks each with a length of 5 days, we randomly sample 10 chunks of 5 consecutive days. We assign a phase value to each of these randomly selected days based on the phase value of the true events. For example, if the first of the true MJO events of length five are made up of three consecutive days in phase 3 and then two days in phase 4, then our randomly selected data will be given the same phase values. Selecting our random samples in this way ensures that the autocorrelations between and within phase values are retained. Next, only the indices of true MJO days whose amplitudes are greater than 1 are used to construct the composites making up the bootstrap samples. As in the composites of observed data, we use independent random days that have been selected in the same manner as described previously, and construct 500 2-D bootstrap composites for each weather station and variable. Finally, we calculate the STRIPES index for each of the bootstrap composites to create a distribution of STRIPES indices that can arise due to random chance. Those stations with a STRIPES index larger than the 95th percentile of their respective distribution are considered significant.

Acknowledgments
This research has been supported by NSF grant AGS-1445191 to Colorado State University. This research was also conducted as part of the NOAA MAPP S2S Prediction Task Force by supporting E. A. B. on NOAA grant NA16OAR4310064. NCEP/NCAR Reanalysis data are provided by the NOAA/OAR/ESRL PSD, Boulder, Colorado, USA (https://www.esrl.noaa.gov/psd/). Station data are from the Global Historical Climatology Network-Daily database, provided by the NOAA/NCEI (http://www1.ncdc.noaa.gov/pub/data/ghcn/daily). RMM MJO data are provided by the Australian Bureau of Meteorology (http://www.bom.gov.au/climate/mjo/graphics/rmm.74toRealtime.txt).

References

Baggett, C. F., Barnes, E. A., Maloney, E. D., & Mundhenk, B. D. (2017). Advancing atmospheric river forecasts into subseasonal-to-seasonal time scales: Forecasting ARs at S2S time scales. *Geophysical Research Letters*, *44*, 7528–7536. https://doi.org/10.1002/2017GL074434

Baxter, S., Weaver, S., Gottschalck, J., & Xue, Y. (2014). Pentad evolution of wintertime impacts of the Madden–Julian Oscillation over the contiguous United States. *Journal of Climate*, *27*(19), 7356–7367. https://doi.org/10.1175/JCLI-D-14-00105.1

Becker, E. J., Berbery, E. H., & Higgins, R. W. (2011). Modulation of cold-season U.S. daily precipitation by the Madden-Julian oscillation. *Journal of Climate*, *24*(19), 5157–5166. https://doi.org/10.1175/2011JCLI4018.1

Black, J., Johnson, N. C., Baxter, S., Feldstein, S. B., Harnos, D. S., & L'Heureux, M. L. (2017). The predictors and forecast skill of Northern Hemisphere teleconnection patterns for lead times of 3–4 weeks. *Monthly Weather Review*, *145*(7), 2855–2877. https://doi.org/10.1175/MWR-D-16-0394.1

Bond, N. A., & Vecchi, G. A. (2003). The influence of the Madden–Julian Oscillation on precipitation in Oregon and Washington. *Weather Forecast*, *18*(4), 600–613. https://doi.org/10.1175/1520-0434(2003)018<0600:TIOTMO>2.0.CO;2

Cassou, C. (2008). Intraseasonal interaction between the Madden-Julian Oscillation and the North Atlantic Oscillation. *Nature*, *455*(7212), 523–527. https://doi.org/10.1038/nature07286

Curtis, S., & Gamble, D. W. (2016). The boreal winter Madden-Julian Oscillation's influence on summertime precipitation in the greater Caribbean. *Journal of Geophysical Research: Atmospheres*, *121*, 7592–7605. https://doi.org/10.1002/2016JD025031

DelSole, T., Trenary, L., Tippett, M. K., & Pegion, K. (2017). Predictability of Week-3–4 average temperature and precipitation over the Contiguous United States. *Journal of Climate*, *30*(10), 3499–3512. https://doi.org/10.1175/JCLI-D-16-0567.1

Diao, Y., Li, T., & Hsu, P. C. (2018). Influence of the boreal summer intraseasonal oscillation on extreme temperature events in the Northern Hemisphere. *Journal of Meteorological Research*, *32*, 534–547.

Donald, A., Meinke, H., Power, B., Maia, A. d. H. N., Wheeler, M. C., White, N., & Ribbe, J. (2006). Near-global impact of the Madden-Julian Oscillation on rainfall. *Geophysical Research Letters*, *33*, L09704. https://doi.org/10.1029/2005GL025155

Ferranti, L., Palmer, T. N., Molteni, F., & Klinker, E. (1990). Tropical-extratropical interaction associated with the 30–60 day oscillation and its impact on medium and extended range prediction. *Journal of the Atmospheric Sciences*, *47*(18), 2177–2199. https://doi.org/10.1175/1520-0469(1990)047<2177:TEIAWT>2.0.CO;2

Garfinkel, C. I., Feldstein, S. B., Waugh, D. W., Yoo, C., & Lee, S. (2012). Observed connection between stratospheric sudden warmings and the Madden-Julian Oscillation. *Geophysical Research Letters*, *39*, L18807. https://doi.org/10.1029/2012GL053144

Goss, M., & Feldstein, S. B. (2015). The impact of the initial flow on the extratropical response to Madden–Julian Oscillation convective heating. *Monthly Weather Review*, *143*(4), 1104–1121. https://doi.org/10.1175/MWR-D-14-00141.1

Hartmann, D. L. (1994). *Global physical climatology*. San Diego, CA: Academic Press.

He, J., Lin, H., & Wu, Z. (2011). Another look at influences of the Madden-Julian Oscillation on the wintertime East Asian weather. *Journal of Geophysical Research*, *116*, D03109. https://doi.org/10.1029/2010JD014787

Henderson, S. A., & Maloney, E. D. (2018). The impact of the Madden–Julian Oscillation on high-latitude winter blocking during El Niño–Southern Oscillation events. *Journal of Climate*, *31*(13), 5293–5318. https://doi.org/10.1175/JCLI-D-17-0721.1

Henderson, S. A., Maloney, E. D., & Barnes, E. A. (2016). The influence of the Madden-Julian oscillation on Northern Hemisphere winter blocking. *Journal of Climate*, *29*(12), 4597–4616. https://doi.org/10.1175/JCLI-D-15-0502.1

Hendon, H. H., & Salby, M. L. (1994). The life cycle of the Madden–Julian Oscillation. *Journal of the Atmospheric Sciences*, *51*(15), 2225–2237. https://doi.org/10.1175/1520-0469(1994)051<2225:TLCOTM>2.0.CO;2

Higgins, R. W., & Mo, K. C. (1997). Persistent North Pacific circulation anomalies and the tropical intraseasonal oscillation. *Journal of Climate*, *10*(2), 223–244. https://doi.org/10.1175/1520-0442(1997)010<0223:PNPCAA>2.0.CO;2

Hoskins, B. J. (2013). The potential for skill across the range of the seamless weather-climate prediction problem: A stimulus for our science. *Quarterly Journal of the Royal Meteorological Society*, *139*(672), 573–584. https://doi.org/10.1002/qj.1991

Hoskins, B. J., & Karoly, D. J. (1981). The steady linear response of a spherical atmosphere to thermal and orographic forcing. *Journal of the Atmospheric Sciences*, *38*(6), 1179–1196. https://doi.org/10.1175/1520-0469(1981)038<1179:TSLROA>2.0.CO;2

Hudson, D., Marshall, A. G., Alves, O., Young, G., Jones, D., & Watkins, A. (2015). Forewarned is forearmed: Extended-range forecast guidance of recent extreme heat events in Australia. *Weather Forecasting*, *31*(3), 697–711. https://doi.org/10.1175/WAF-D-15-0079.1

James, W. E. (1953). Forecasting ground frost. *Meteorological Magazine*, *82*(969), 91.

Johansson, Å. (2007). Prediction skill of the NAO and PNA from daily to seasonal time scales. *Journal of Climate*, *20*(10), 1957–1975. https://doi.org/10.1175/JCLI4072.1

Johnson, N. C., Collins, D. C., Feldstein, S. B., L'Heureux, M. L., & Riddle, E. E. (2014). Skillful wintertime North American temperature forecasts out to 4 weeks based on the state of ENSO and the MJO*. *Weather Forecasting*, *29*(1), 23–38. https://doi.org/10.1175/WAF-D-13-00102.1

Johnson, N. C., & Feldstein, S. B. (2010). The continuum of North Pacific Sea level pressure patterns: Intraseasonal, interannual, and interdecadal variability. *Journal of Climate*, *23*(4), 851–867. https://doi.org/10.1175/2009JCLI3099.1

Jones, C., & Carvalho, L. M. V. (2014). Sensitivity to Madden–Julian Oscillation variations on heavy precipitation over the contiguous United States. *Atmospheric Research*, *147-148*, 10–26. https://doi.org/10.1016/j.atmosres.2014.05.002

Jones, C., Gottschalck, J., Carvalho, L. M. V., & Higgins, W. (2011). Influence of the Madden–Julian Oscillation on forecasts of extreme precipitation in the Contiguous United States. *Monthly Weather Review*, *139*(2), 332–350. https://doi.org/10.1175/2010MWR3512.1

Jones, C., Waliser, D. E., Lau, K. M., & Stern, W. (2004). Global occurrences of extreme precipitation and the Madden–Julian Oscillation: Observations and predictability. *Journal of Climate*, *17*(23), 4575–4589. https://doi.org/10.1175/3238.1

Kalnay, E., Kanamitsu, M., Kistler, R., Collins, W., Deaven, D., Gandin, L., & Joseph, D. (1996). The NCEP/NCAR 40-year reanalysis project. *Bulletin of the American Meteorological Society*, *77*(3), 437–472. https://doi.org/10.1175/1520-0477(1996)077<0437:TNYRP>2.0.CO;2

Limpasuvan, V., Thompson, D. W. J., & Hartmann, D. L. (2004). The life cycle of the Northern Hemisphere sudden stratospheric warmings. *Journal of Climate*, *17*(13), 2584–2596. https://doi.org/10.1175/1520-0442(2004)017<2584:TLCOTN>2.0.CO;2

Lin, H., Brunet, G., & Derome, J. (2009). An observed connection between the North Atlantic Oscillation and the Madden–Julian Oscillation. *Journal of Climate*, *22*(2), 364–380. https://doi.org/10.1175/2008JCLI2515.1

Lin, H., Brunet, G., & Fontecilla, J. S. (2010b). Impact of the Madden-Julian Oscillation on the intraseasonal forecast skill of the North Atlantic Oscillation. *Geophysical Research Letters*, *37*, L19803. https://doi.org/10.1029/2010GL044315

Lin, H., Brunet, G., & Mo, R. (2010a). Impact of the Madden–Julian Oscillation on wintertime precipitation in Canada. *Monthly Weather Review*, *138*(10), 3822–3839. https://doi.org/10.1175/2010MWR3363.1

Madden, R. A., & Julian, P. R. (1971). Detection of a 40–50 day oscillation in the zonal wind in the tropical Pacific. *Journal of Atmospheric Sciences*, *28*(5), 702–708. https://doi.org/10.1175/1520-0469(1971)028<0702:DOADOI>2.0.CO;2

Madden, R. A., & Julian, P. R. (1972). Description of global-scale circulation cells in the tropics with a 40–50 day period. *Journal of Atmospheric Sciences*, *29*(6), 1109–1123. https://doi.org/10.1175/1520-0469(1972)029<1109:DOGSCC>2.0.CO;2

Mariotti, A., Ruti, P. M., & Rixen, M. (2018). Progress in subseasonal to seasonal prediction through a joint weather and climate community effort. *Climate and Atmospheric Science*, *1*(1), 4. https://doi.org/10.1038/s41612-018-0014-z

Matsueda, S., & Takaya, Y. (2015). The global influence of the Madden–Julian Oscillation on extreme temperature events. *Journal of Climate*, *28*, 4141–4151. https://doi.org/10.1175/JCLI-D-14-00625.1

McKinnon, K. A., Rhines, A., Tingley, M. P., & Huybers, P. (2016). Long-lead predictions of eastern United States hot days from Pacific sea surface temperatures. *Nature Geoscience*, *9*(5), 389–394. https://doi.org/10.1038/ngeo2687

Menne, M. J., Durre, I., Vose, R. S., Gleason, B. E., & Houston, T. G. (2012). An overview of the global historical climatology network-daily database. *Journal of Atmospheric and Oceanic Technology*, *29*(7), 897–910. https://doi.org/10.1175/JTECH-D-11-00103.1

Mo, K. C., & Higgins, R. W. (1998). Tropical convection and precipitation regimes in the Western United States. *Journal of Climate*, *11*(9), 2404–2423.

Moon, J. Y., Wang, B., & Ha, K. J. (2011). ENSO regulation of MJO teleconnection. *Climate Dynamics*, *37*(5), 1133–1149. https://doi.org/10.1007/s00382-010-0902-3

Moon, J. Y., Wang, B., Ha, K. J., & Lee, J. Y. (2013). Teleconnections associated with Northern Hemisphere summer monsoon intraseasonal oscillation. *Climate Dynamics*, *40*(11), 2761–2774. https://doi.org/10.1007/s00382-012-1394-0

Moore, R. W., Martius, O., & Spengler, T. (2010). The modulation of the subtropical and extratropical atmosphere in the Pacific basin in response to the Madden–Julian Oscillation. *Monthly Weather Review*, *138*(7), 2761–2779. https://doi.org/10.1175/2010MWR3194.1

Mori, M., & Watanabe, M. (2008). The growth and triggering mechanisms of the PNA: A MJO-PNA coherence. *Journal of the Meteorological Society of Japan*, *86*(1), 213–236. https://doi.org/10.2151/jmsj.86.213

Mundhenk, B. D., Barnes, E. A., & Maloney, E. D. (2016). All-season climatology and variability of atmospheric river frequencies over the North Pacific. *Journal of Climate*, *29*(13), 4885–4903. https://doi.org/10.1175/JCLI-D-15-0655.1

Mundhenk, B. D., Barnes, E. A., Maloney, E. D., & Baggett, C. F. (2018). Skillful empirical subseasonal prediction of landfalling atmospheric river activity using the Madden–Julian oscillation and quasi-biennial oscillation. *Climate and Atmospheric Science*, *1*(1), 7. https://doi.org/10.1038/s41612-017-0008-2

Ralph, F. M., Neiman, P. J., Kiladis, G. N., & Weickmann, K. (2010). A multiscale observational case study of a Pacific atmospheric river exhibiting tropical–extratropical connections and a mesoscale frontal wave. *Monthly Weather Review*, *139*(4), 1169–1189. https://doi.org/10.1175/2010MWR3596.1

Riddle, E. E., Stoner, M. B., Johnson, N. C., L'Heureux, M. L., Collins, D. C., & Feldstein, S. B. (2013). The impact of the MJO on clusters of wintertime circulation anomalies over the North American region. *Climate Dynamics*, *40*(7-8), 1749–1766. https://doi.org/10.1007/s00382-012-1493-y

Roundy, P. E., MacRitchie, K., Asuma, J., & Melino, T. (2010). Modulation of the global atmospheric circulation by combined activity in the Madden-Julian oscillation and the El Niño–outhern Oscillation during boreal winter. *Journal of Climate*, *23*(15), 4045–4059. https://doi.org/10.1175/2010JCLI3446.1

Schreck, C. J., Cordeira, J. M., & Margolin, D. (2013). Which MJO events affect North American temperatures? *Monthly Weather Review*, *141*(11), 3840–3850. https://doi.org/10.1175/MWR-D-13-00118.1

Seo, K. H., & Lee, H. J. (2017). Mechanisms for a PNA-like teleconnection pattern in response to the MJO. *Journal of the Atmospheric Sciences*, *74*(6), 1767–1781. https://doi.org/10.1175/JAS-D-16-0343.1

Seo, K. H., Lee, H. J., & Frierson, D. M. W. (2016). Unraveling the teleconnection mechanisms that induce wintertime temperature anomalies over the Northern Hemisphere continents in response to the MJO. *Journal of the Atmospheric Sciences*, *73*(9), 3557–3571. https://doi.org/10.1175/JAS-D-16-0036.1

Slade, S. A., & Maloney, E. D. (2013). An intraseasonal prediction model of Atlantic and East Pacific tropical cyclone genesis. *Monthly Weather Review*, *141*(6), 1925–1942. https://doi.org/10.1175/MWR-D-12-00268.1

Son, S. W., Lim, Y., Yoo, C., Hendon, H. H., & Kim, J. (2017). Stratospheric control of the Madden–Julian Oscillation. *Journal of Climate*, *30*(6), 1909–1922. https://doi.org/10.1175/JCLI-D-16-0620.1

Vitart, F., Ardilouze, C., Bonet, A., Brookshaw, A., Chen, M., Codorean, C., & Zhang, L. (2017). The subseasonal to seasonal (S2S) prediction project database. *Bulletin of the American Meteorological Society*, *98*(1), 163–173. https://doi.org/10.1175/BAMS-D-16-0017.1

Vitart, F., & Molteni, F. (2010). Simulation of the Madden–Julian Oscillation and its teleconnections in the ECMWF forecast system. *Quarterly Journal of the Royal Meteorological Society*, *136*(649), 842–855. https://doi.org/10.1002/qj.623

Wheeler, M. C., & Hendon, H. H. (2004). An all-season real-time multivariate MJO index: Development of an Index for monitoring and prediction. *Monthly Weather Review*, *132*(8), 1917–1932. https://doi.org/10.1175/1520-0493(2004)132<1917:AARMMI>2.0.CO;2

White, C. J., Carlsen, H., Robertson, A. W., Klein, R. J. T., Lazo, J. K., Kumar, A., & Zebiak, S. E. (2017). Potential applications of subseasonal-to-seasonal (S2S) predictions. *Meteorological Applications*, *24*(3), 315–325. https://doi.org/10.1002/met.1654

Zhang, C. (2013). Madden-Julian oscillation: Bridging weather and climate. *Bulletin of the American Meteorological Society*, *94*(12), 1849–1870. https://doi.org/10.1175/BAMS-D-12-00026.1

Zheng, C., Kar-Man Chang, E., Kim, H. M., Zhang, M., & Wang, W. (2018). Impacts of the Madden–Julian oscillation on storm-track activity, surface air temperature, and precipitation over North America. *Journal of Climate*, *31*(15), 6113–6134. https://doi.org/10.1175/JCLI-D-17-0534.1

Zhou, S., L'Heureux, M., Weaver, S., & Kumar, A. (2012). A composite study of the MJO influence on the surface air temperature and precipitation over the Continental United States. *Climate Dynamics*, *38*(7-8), 1459–1471. https://doi.org/10.1007/s00382-011-1001-9

Zhu, Z., & Li, T. (2017). The statistical extended-range (10–30-day) forecast of summer rainfall anomalies over the entire China. *Climate Dynamics*, *48*(1), 209–224. https://doi.org/10.1007/s00382-016-3070-2